Original Article | Breast Imaging

eISSN 2005-8330
https://doi.org/10.3348/kjr.2019.0567
Korean J Radiol 2020;21(5):561-571

Korean Journal of Radiology
KJR

Ultrafast Dynamic Contrast-Enhanced Breast MRI: Lesion Conspicuity and Size Assessment according to Background Parenchymal Enhancement

Soo-Yeon Kim, MD, PhD[1, 2, 3], Nariya Cho, MD, PhD[1, 2, 3], Yunhee Choi, PhD[4], Sung Ui Shin, MD, PhD[1, 2, 3, 5], Eun Sil Kim, MD[1, 2, 3], Su Hyun Lee, MD, PhD[1, 2, 3], Jung Min Chang, MD, PhD[1, 2, 3], Woo Kyung Moon, MD, PhD[1, 2, 3]

[1]Department of Radiology, Seoul National University Hospital, Seoul, Korea; [2]Department of Radiology, Seoul National College of Medicine, Seoul, Korea; [3]Institute of Radiation Medicine, Seoul National University Medical Research Center, Seoul, Korea; [4]Medical Research Collaborating Center, Seoul National University Hospital, Seoul, Korea; [5]Department of Radiology, Seoul National University Hospital Healthcare System Gangnam Center, Seoul, Korea

Objective: To evaluate the clinical utility of ultrafast dynamic contrast-enhanced (DCE)-MRI compared to conventional DCE-MRI by studying lesion conspicuity and size according to the level of background parenchymal enhancement (BPE).

Materials and Methods: This study included 360 women (median age, 54 years; range, 26–82 years) with 361 who had undergone breast MRI, including both ultrafast and conventional DCE-MRI before surgery, between January and December 2017. Conspicuity was evaluated using a five-point score. Size was measured as the single maximal diameter. The Wilcoxon signed-rank test was used to compare median conspicuity score. To identify factors associated with conspicuity, multivariable logistic regression was performed. Absolute agreement between size at MRI and histopathologic examination was assessed using the intraclass correlation coefficient (ICC).

Results: The median conspicuity scores were 5 at both scans, but the interquartile ranges were significantly different (5-5 at ultrafast vs. 4-5 at conventional, $p < 0.001$). Premenopausal status (odds ratio [OR] = 2.2, $p = 0.048$), non-mass enhancement (OR = 4.1, $p = 0.001$), moderate to marked BPE (OR = 7.5, $p < 0.001$), and shorter time to enhancement (OR = 0.9, $p = 0.043$) were independently associated with better conspicuity at ultrafast scans. Tumor size agreement between MRI and histopathologic examination was similar for both scans (ICC = 0.66 for ultrafast vs. 0.63 for conventional).

Conclusion: Ultrafast DCE-MRI could improve lesion conspicuity compared to conventional DCE-MRI, especially in women with premenopausal status, non-mass enhancement, moderate to marked BPE or short time to enhancement.

Keywords: *Ultrafast breast dynamic contrast-enhanced MRI; Lesion conspicuity; Lesion size; Background parenchymal enhancement; Breast cancer*

INTRODUCTION

Breast ultrafast dynamic contrast-enhanced (DCE)-MRI takes multiple images before the first post-contrast phase of conventional DCE-MRI (1-13). High spatiotemporal resolution can be achieved with the use of various acceleration techniques, such as view-sharing, parallel imaging or compressed sensing (1-10). The view-sharing technique used in the present study heavily undersamples the outer part of the k-space but shares data between successive time points (1). In the compressed sensing technique, a subset of the full k-space is acquired through

Received August 2, 2019; accepted after revision January 13, 2020.
This study has received funding by grant (no.04-2017-0470) from the Seoul National University Hospital Research Fund.
Corresponding author: Nariya Cho, MD, PhD, Department of Radiology, Seoul National University College of Medicine, 101 Daehak-ro, Jongno-gu, Seoul 03080, Korea.
• Tel: (822) 2072-1862 • Fax: (822) 743-6385 • E-mail: river7774@gmail.com

random sampling (5). Several studies have reported that the initial enhancement analysis results obtained from ultrafast DCE-MRI such as maximum slope and time to enhancement (TTE) show non-inferior accuracy in discriminating benign breast lesions from malignant lesions compared to the Breast Imaging Reporting and Data System (BI-RADS) curve analysis results obtained through conventional DCE-MRI (1, 2), although further validation is needed. Diagnostic accuracy was also improved when data from the initial enhancement analysis was combined with conventional BI-RADS categorization, compared with BI-RADS alone, especially for non-mass breast lesions (3). Moreover, screening results using breast ultrafast DCE-MRI showed higher specificity, shorter reading times, and non-inferior accuracy compared to full diagnostic MRI (4).

Although background parenchymal enhancement (BPE) on breast MRI results from physiological enhancement in fibroglandular tissue, strong BPE may yield abnormal interpretation and false-positive biopsy results (14, 15). Moderate to marked BPE is also associated with an inaccurate estimation of tumor size at preoperative staging MRI and has been associated with higher rates of positive resection margins (16-20). In general, BPE increases after a contrast agent is administered and is more prominent during the late phase than the early phase in DCE-MRI (19). Compared to conventional DCE-MRI, BPE may be attenuated in ultrafast DCE-MRI, because images are obtained before the first post-contrast phase of conventional DCE-MRI, and normal fibroglandular tissue needs more time for sufficient enhancement compared to a tumor (8, 21). Due to this attenuated BPE, ultrafast DCE-MRI may show better performance in the assessment of lesion conspicuity and tumor size than conventional DCE-MRI, especially for women with moderate to marked BPE on conventional DCE-MRI.

Thus, the aims of the present study were to evaluate the clinical utility of ultrafast DCE-MRI compared to conventional DCE-MRI through the evaluation of breast lesion conspicuity and tumor size according to the level of BPE.

MATERIALS AND METHODS

Patient Selection

Our retrospective study was approved by the Institutional Review Board, and the requirement for informed consent was waived. From the breast MRI database, we identified 718 consecutive breast cancer patients who had undergone preoperative breast MRI examinations with a combined protocol, including ultrafast and conventional DCE-MRI and subsequent surgery, between January and December 2017. The exclusion criteria excluded patients who had undergone neoadjuvant chemotherapy (n = 132), multiple lesions at surgical histopathology (n = 117), vacuum or surgical excision prior to the MRI (n = 99), or recurrence at the chest wall or axilla (n = 9). Women who had undergone neoadjuvant chemotherapy were excluded because recent studies show that the delayed phase of conventional DCE-MRI provides more accurate measurements for tumor size than the early phase in this population; as ultrafast DCE-MRI is performed even earlier in these patients, its assessments may be inaccurate for residual cancer after chemotherapy (22, 23). Women with multiple lesions at surgical pathological examination were excluded because one-to-one matching between MRI-identified lesions and pathology-diagnosed lesions was not feasible in most cases. Finally, 360 women (median age, 54 years; range, 26–82 years) with 361 tumors were included. One woman had bilateral breast cancers. The median interval between MRI and surgery was 9 days (range, 1–65 days; interquartile range, 1–21 days).

MRI Protocol

All patients were scanned in the prone position using a 3T MRI scanner (Ingenia, Philips Healthcare, Best, the Netherlands [n = 237, 66%] or Skyra, Siemens Healthineers, Erlangen, Germany [n = 123, 34%]) with a 16-channel bilateral breast coil. The dynamic series were preceded by an axial T2-weighted sequence followed by a sagittal T1-weighted sequence, an axial T1-weighted sequence for axillary regions, and an axial diffusion-weighted sequence. Immediately after acquisition with the conventional, pre-contrast, axial T1-weighted spoiled gradient echo sequence using volume-interpolated breath-hold examination (VIBE) or enhanced-T1 high-resolution isotropic volume examination (eTHRIVE), a series of 20 ultrafast acquisitions were interleaved before the first post-contrast phase of conventional DCE-MRI (Fig. 1). Time-resolved angiography with stochastic trajectories (TWIST) or four dimensional time-resolved angiography with keyhole (4D-TRAK) techniques were used for the ultrafast DCE-MRI. Of the 20 ultrafast series, the first three were obtained before contrast injection, and the subsequent 17 series were obtained immediately after and during contrast injection. An intravenous bolus of gadobutrol (Gadovist, Bayer

https://doi.org/10.3348/kjr.2019.0567

Korean Journal of Radiology
KJR

Healthcare, Berlin, Germany) was administered with a power injector (Spectris Solaris, Medrad Europe BV, Maastricht, the Netherlands) at a dose of 0.1 mmol/kg of body weight and at a rate of 2 mL/sec, followed by a 20 mL saline flush. Detailed information for the two dynamic series is provided in Table 1. The time interval from contrast administration until the center of the k-space of the first post-contrast conventional series was 109.4 seconds for Siemens VIBE and 149.5 seconds for Philips eTHRIVE.

Data Analysis

Medical records were reviewed to collect clinical-pathologic data, including age, menopausal status, tumor, node, and metastasis (TNM) stage, histological type, histological grade of invasive cancer, nuclear grade of ductal carcinoma *in situ* (DCIS), tumor size at surgical histopathological examination, and estrogen receptor (ER), progesterone receptor (PR), and human epidermal growth factor receptor 2 (HER2) status (24, 25). Positive ER and PR expression were defined as nuclear staining ≥ 1% of tumor cells, using standard immunohistochemistry methods. Hormone receptor (HR) positivity was defined as ER and/or PR positivity. Positive HER2 expression was defined by a score of 3+ or gene amplification by fluorescence *in*

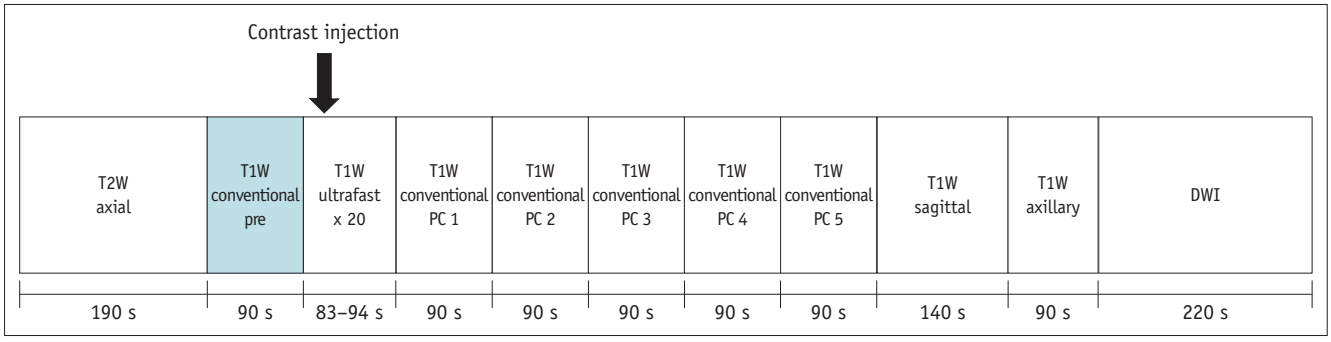

Fig. 1. Combined DCE-MRI protocol used in our study. DCE = dynamic contrast-enhanced, DWI = diffusion-weighted imaging, PC = post-contrast, s = seconds, T1W = T1-weighted, T2W = T2-weighted

Table 1. Combined Breast DCE-MRI Protocol

Vendors	Skyra (Siemens)		Ingenia (Philips)	
Techniques	Ultrafast	Conventional	Ultrafast	Conventional
Sequence name	TWIST	VIBE	4D-TRAK	eTHRIVE
View sharing (%)				
Central zone	18	NA	50	NA
Sampling density outer zone	10	NA	NA	NA
Parallel imaging factor	CAIPIRINHA: 5	CAIPIRINHA: 2 GRAPPA: 2	SENSE: 4 (phase direction) 2 (slice direction)	SENSE: 3.2 (phase direction) 1 (slice direction)
Number of dynamics	20 (3 pre, 17 post)	6 (1 pre, 5 post)	20 (3 pre, 17 post)	6 (1 pre, 5 post)
Temporal resolution (sec)	3.8	88	4.5	89
Spatial resolution (mm)	1.1 x 1.1 x 1.0	0.8 x 0.8 x 1.0	1.0 x 1.0 x 1.0	0.9 x 0.9 x 1.0
Field of view (mm)	320	320	300	300
Number of slices	144	144	160	160
TE/TR (msec)	2.6/4.1	1.7/4.7	2.0/3.9	1.8/4.1
Flip angle	10	10	12	12
Fat suppression	DIXON	SPAIR	SPAIR	SPAIR

First series of ultrafast DCE-MRI needed 11 seconds for TWIST and 9 seconds for 4D-TRAK to obtain full k-space, and subsequent 19 series took 3.8 seconds for TWIST and 4.5 seconds for 4D-TRAK per series. Total acquisition time was 83.2 seconds for TWIST and 94.5 seconds for 4D-TRAK. CAIPIRINHA = controlled aliasing in parallel imaging results in higher acceleration, DCE = dynamic contrast-enhanced, eTHRIVE = enhanced-T1 high-resolution isotropic volume examination, GRAPPA = generalized autocalibrating partial parallel acquisition, NA = not applicable, SENSE = sensitivity encoding, SPAIR = spectral attenuated inversion recovery, TE = echo time, TR = repetition time, TWIST = time-resolved angiography with stochastic trajectories, VIBE = volume-interpolated breath-hold examination, 4D-TRAK = four dimensional time-resolved angiography with keyhole

https://doi.org/10.3348/kjr.2019.0567

situ hybridization in tumors with a score of 2+. The tumor subtypes were categorized as follows: HR-positive/HER2-negative, HR-positive/HER2-positive, HR-negative/HER2-positive, or triple-negative (ER-, PR-, and HER2-negative).

Image Analysis

Lesion conspicuity was evaluated by two radiologists dedicated to breast imaging with 6 years and 16 years of experience, respectively, by consensus using a five-point Likert scale as follows: 1, nondiagnostic (impossible to find tumor); 2, poor (reduced contrast preventing distinction of the tumor from BPE across at least 50% of the tumor margin); 3, acceptable (tumor/BPE generally identifiable but with a significant loss of contrast that prevents clear tumor margins); 4, good (well-defined tumor/BPE boundaries over at least 50% of the tumor); and 5, excellent (well-defined tumor/BPE boundaries in the entire breast). Readings for lesion conspicuity were divided into two sessions, with cases being divided into two equal groups after being lined up in consecutive order according to the time of MRI acquisition. In the first reading session, ultrafast images were reviewed for the first group of cases to undergo MRI acquisition, and conventional images were reviewed for the second group. After one month, in the second reading session, ultrafast images were reviewed for the second group, and conventional images were reviewed for the first group.

One month after reviewing lesion conspicuity, the tumor size which was defined by the single largest diameter of the enhancing tumor, was measured on each MRI scan by the two radiologists by consensus. First, ultrafast images were reviewed for all cases. After one month, conventional images were reviewed for all cases. To determine appropriate time points for measuring tumor size with ultrafast MRI, we first set up the following four time points (Fig. 2): U1, the time point at which the tumor begins to become enhanced; U2, the subsequent time point after the tumor begins to become enhanced; U3, the middle time point after contrast injection (12th); U4, the last time point of the ultrafast sequence (20th). Thereafter, we measured 30 tumor cases at each time point of the ultrafast MRI. With conventional DCE-MRI, each tumor was evaluated at the first post-contrast images to minimize BPE. Lesion type (mass and non-mass enhancement [NME]) and BPE (minimal, mild, moderate, and marked) were also analyzed at the first post-contrast images of conventional DCE-MRI according to BI-RADS (14). In regard to lesion type, masses with accompanying NME were interpreted as the NME type. On ultrafast DCE-MRI, TTE was defined as the time interval from when the aorta started to enhance to when the tumor started to enhance (2). In our study, it was calculated by the phase of the initial enhancement of the tumor relative to the ascending aorta, multiplied by the temporal resolution, which was 3.8 seconds for TWIST and 4.5 seconds for 4D-TRAK. The kinetic curve pattern of the initial phase and delayed phase of conventional DCE-MRI was assessed according to BI-RADS (14).

Statistical Analysis

The Wilcoxon singed-rank test was used to compare the median conspicuity score and median tumor size between MRI scans. To identify factors associated with better conspicuity scores at ultrafast DCE-MRI, univariable and multivariable logistic regression analyses were performed. Absolute size agreements between surgical histopathological examination and MRI were evaluated using the intraclass correlation coefficient (ICC) analysis (two-way mixed model, absolute agreement definition, and a single measure). ICC values according to DCE-MRI method and BPE were compared using Fisher's Z-test. To identify the factors affecting the size discrepancy between pathology and MRI, simple and multiple linear regression analyses were performed. SPSS software (PASW Statistics, version 21, IBM Corp., Armonk, NY, USA) was used for the statistical analysis. A p value < 0.05 was considered statistically significant.

RESULTS

Patient Characteristics

Patient characteristics are presented in Table 2. At the first post-contrast phase of conventional DCE-MRI, 252 (69.8%) patients had minimal to mild BPE, and 109 (30.2%) patients had moderate to marked BPE. Premenopausal women showed moderate to marked BPE more frequently than postmenopausal women did (55.0% [82 of 149] vs. 12.7% [27 of 212], respectively, p < 0.001).

Comparison of Lesion Conspicuity Scores

The median lesion conspicuity scores at both ultrafast and conventional DCE-MRI were the same at 5, but the interquartile ranges were significantly different (5-5 at ultrafast vs. 4-5 at conventional, p < 0.001). Most cases (79.7%, 288 of 361) showed the same conspicuity scores for ultrafast and conventional DCE-MRI. Sixty-one (16.9%)

https://doi.org/10.3348/kjr.2019.0567

Korean Journal of Radiology
KJR

cases showed higher conspicuity scores and 12 (3.3%) cases showed lower conspicuity scores at ultrafast DCE-MRI than at conventional DCE-MRI. There were significantly more cases with better conspicuity scores at ultrafast DCE-MRI than at conventional DCE-MRI (16.9% vs. 3.3%, respectively, $p < 0.001$). According to multivariable logistic regression analysis, premenopausal status (odds ratio [OR] = 2.2, $p = 0.048$), NME (OR = 4.1, $p = 0.001$), moderate to marked BPE (OR = 7.5, $p < 0.001$), and shorter TTE (OR = 0.9, $p = 0.043$) were independently associated with better

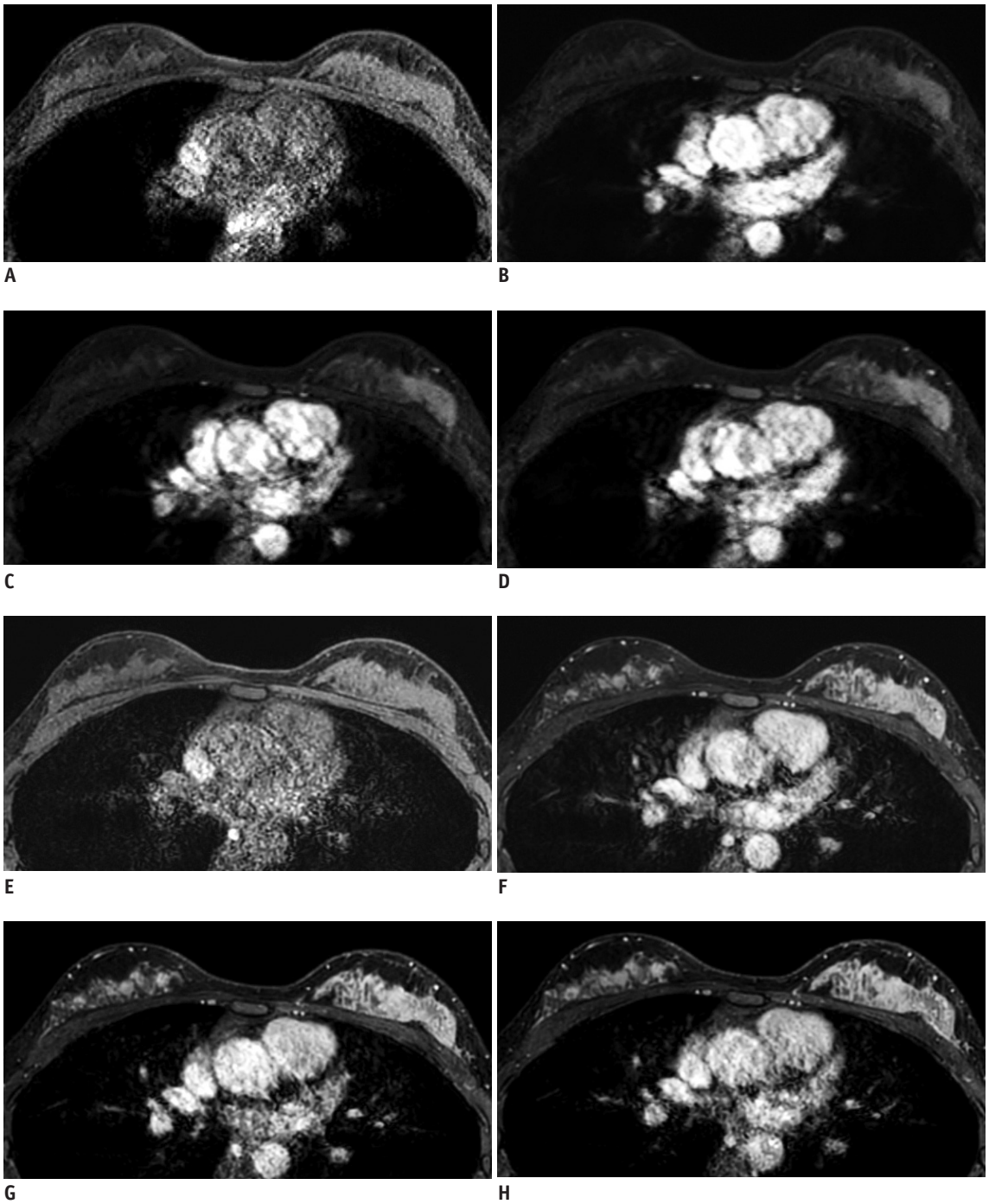

Fig. 2. Representative example of four time points of ultrafast (A-D) and conventional (E-H) DCE-MRI. This case was scanned using Skyra (Siemens Healthineers). **A.** Pre-contrast image. **B.** U1, time point when tumor begins to become enhanced, 7th phase in this case. **C.** U2, subsequent time point when tumor begins to become enhanced, 8th phase in this case. **D.** U3, middle time point after contrast injection, 12th phase in this case. Pre-contrast **(E)**, first **(F)**, third **(G)**, and fifth **(H)** post-contrast phases of conventional DCE-MRI. Lesion conspicuity scores and size measurements were performed at U2 **(B)** of ultrafast scans and at first post-contrast phase **(F)** of conventional scans.

https://doi.org/10.3348/kjr.2019.0567

Table 2. Patient and Tumor Characteristics

Characteristics	Data
Age (years)	
Mean ± standard deviation	54.7 ± 11.2
Median (ranges)	54 (26–82)
Menopausal status	
Premenopausal	149 (41.3)
Postmenopausal	212 (58.7)
TNM stages	
0	49 (13.6)
I	176 (48.7)
II	122 (33.8)
III	14 (3.9)
Histologic types	
DCIS	49 (13.6)
Invasive ductal carcinoma, not otherwise specified	276 (76.5)
Invasive lobular carcinoma	19 (5.3)
Mucinous carcinoma	12 (3.3)
Invasive papillary carcinoma	3 (0.8)
Invasive cribriform carcinoma	1 (0.3)
Metaplastic carcinoma	1 (0.3)
Histologic or nuclear grades	
Low	54 (15.0)
Intermediate	207 (57.3)
High	100 (27.7)
Tumor subtypes	
HR+/HER2-	236 (65.4)
HR+/HER2+	31 (8.6)
HR-/HER2+	44 (12.2)
Triple negative	50 (13.9)
Tumor size at surgical histopathologic examination (cm)*	2.5 (1.9–3.7)
Tumor size at ultrafast DCE-MRI (cm)*	1.9 (1.3–3.3)
Tumor size at conventional DCE-MRI (cm)*	2.1 (1.5–3.3)
Lesion type at MRI	
Mass	288 (79.8)
NME	73 (20.2)
BPE	
Minimal to mild	252 (69.8)
Moderate to marked	109 (30.2)
TTE (seconds)*	9 (7.6–13.5)
Initial phase	
Medium	137 (38.0)
Fast	224 (62.0)
Delayed phase	
Persistent	28 (7.8)
Plateau	153 (42.4)
Washout	180 (49.9)

Data are numbers of patients or tumors, with percentages in parentheses. *Data are medians, with interquartile ranges in parentheses. BPE = background parenchymal enhancement, DCIS = ductal carcinoma *in situ*, HER2 = human epidermal growth factor receptor 2, HR = hormone receptor, NME = non-mass enhancement, TNM = tumor, node, and metastasis, TTE = time to enhancement

conspicuity at ultrafast DCE-MRI than at conventional DCE-MRI (Table 3, Fig. 3). Among 73 NME cases, 21 (28.8%) were DCIS, and 52 (71.2%) were invasive cancers. One DCIS case was not clearly delineated at both ultrafast and conventional DCE-MRI due to lack of enhancement and suspicious features.

Agreement between Histopathological Examination and MRI for Tumor Size according to BPE

To determine appropriate time points for measuring tumor size with ultrafast MRI, the median tumor sizes at U1, U2, U3, and U4 of ultrafast DCE-MRI measured 1.4, 1.5, 1.5, and 1.5 cm, respectively. The median tumor size at U1 was significantly smaller than at U2 (1.4 cm [interquartile range, 0.6–2.1] vs. 1.5 cm [interquartile range, 0.6–2.7], respectively, $p = 0.002$). However, the median tumor sizes at U2-4 were not significantly different from each other (all $p > 0.05$). As BPE usually increases over time after contrast injection, we determined measuring tumor size at U2 was optimal.

Histopathological tumor size was comparable to the tumor size measured by MRI regardless of the chosen DCE-MRI method (ICC = 0.66 for ultrafast vs. 0.63 for conventional, $p = 0.550$). Tumor size measured by ultrafast DCE-MRI was comparable to the histopathological tumor size regardless of BPE (ICC = 0.63 for moderate to marked vs. 0.67 for minimal to mild, $p = 0.338$). Tumor size measured by conventional DCE-MRI was comparable to the histopathological tumor size regardless of BPE (ICC = 0.58 for moderate to marked vs. 0.66 for minimal to mild, $p = 0.067$).

Factors Affecting Size Discrepancy between Pathology and MRI

The multiple linear regression analysis showed that HR+/HER2- subtype ($p = 0.023$), mass type at MRI ($p < 0.001$), and TTE longer than 9 seconds ($p = 0.006$) were independently associated with the size discrepancy between pathology and ultrafast DCE-MRI (Table 4). However, no factor was found to affect size discrepancy between pathology and conventional DCE-MRI (all $p > 0.05$ at the multiple linear regression analysis).

DISCUSSION

Our study found that ultrafast DCE-MRI may improve lesion conspicuity compared to conventional DCE-MRI. Our results are consistent with those of a previous

https://doi.org/10.3348/kjr.2019.0567

Korean Journal of Radiology
KJR

Table 3. Factors Associated with Better Lesion Conspicuity Scores at Ultrafast MRI

Variable	Higher Conspicuity Score at Ultrafast MRI (n = 61)	Similar or Lower Conspicuity Score at Ultrafast MRI (n = 300)	Univariable Odds Ratio (95% CI)	Univariable *P*	Multivariable Odds Ratio (95% CI)	Multivariable *P*
Age (years)				0.166		0.463
< 40 (n = 31)	8 (13.1)	23 (7.7)	1.8 (0.8–4.3)		0.7 (0.2–1.9)	
≥ 40 (n = 330)	53 (86.9)	277 (92.3)	Ref		Ref	
Menopausal status				< 0.001		0.048
Premenopausal (n = 149)	42 (68.9)	107 (35.7)	4.0 (2.2–7.2)		2.2 (1.0–4.7)	
Postmenopausal (n = 212)	19 (31.1)	193 (64.3)	Ref		Ref	
Histologic type				0.053		0.436
DCIS (n = 49)	13 (21.3)	36 (12.0)	2.0 (1.0–4.0)		0.7 (0.3–1.7)	
Invasive carcinoma (n = 312)	48 (78.7)	264 (88.0)	Ref		Ref	
Histologic or nuclear grade				0.778		0.272
Low to intermediate (n = 261)	45 (73.8)	216 (72.0)	Ref		Ref	
High (n = 100)	16 (26.2)	84 (28.0)	0.9 (0.5–1.7)		0.6 (0.3–1.5)	
Tumor subtype				0.917		0.708
HR+/HER2- (n = 236)	42 (68.9)	194 (64.7)	Ref		Ref	
HR+/HER2+ (n = 31)	5 (8.2)	26 (8.7)	0.9 (0.3–2.4)		0.5 (0.1–1.7)	0.281
HR-/HER2+ (n = 44)	6 (9.8)	38 (12.7)	0.7 (0.3–1.8)		1.0 (0.3–3.1)	0.939
Triple negative (n = 50)	8 (13.1)	42 (14.0)	0.9 (0.4–2.0)		1.2 (0.4–3.7)	0.775
Tumor size at histopathologic examination (cm)	2.5 (1.8–4.5)	2.5 (1.9–3.5)	1.1 (0.9–1.3)	0.262	0.9 (0.7–1.1)	0.387
Lesion type at MRI				0.001		0.001
Mass (n = 288)	39 (63.9)	249 (83.0)	Ref		Ref	
NME (n = 73)	22 (36.1)	51 (17.0)	2.8 (1.5–5.0)		4.1 (1.8–9.5)	
BPE at MRI				< 0.001		< 0.001
Minimal to mild (n = 252)	16 (26.2)	236 (78.7)	Ref		Ref	
Moderate to marked (n = 109)	45 (73.8)	64 (21.3)	10.4 (5.5–19.5)		7.5 (3.6–15.6)	
TTE (seconds)	9 (7.6–9.0)	9 (7.6–13.5)	0.9 (0.8–0.9)	0.017	0.9 (0.8–0.9)	0.043
Initial phase				0.363		0.661
Medium (n = 137)	20 (32.8)	117 (39.0)	Ref		Ref	
Fast (n = 224)	41 (67.2)	183 (61.0)	1.3 (0.7–2.3)		1.2 (0.5–2.7)	
Delayed phase				0.439		0.921
Persistent (n = 28)	4 (6.6)	24 (8.0)	Ref		Ref	
Plateau (n = 153)	22 (36.1)	131 (43.7)	1.0 (0.3–3.2)	0.990	0.8 (0.2–3.6)	0.821
Washout (n = 180)	35 (57.4)	145 (48.3)	1.4 (0.5–4.4)	0.517	0.9 (0.2–4.7)	0.969

Categorical data are numbers of tumors, with percentages in parentheses. Continuous data are median, with interquartile ranges in parentheses. CI = confidence interval, Ref = reference standard

study in which lesion conspicuity was highest in the early ultrafast images of cases with marked BPE (8). In that study, researchers quantified the signal intensity changes of cancer, benign lesions, and BPE over time with ultrafast DCE-MRI and found that the lesion-to-background signal intensity ratio was highest during the early ultrafast acquisition and decreased during the final ultrafast acquisition. Furthermore, in cases with marked BPE, maximum conspicuity of the lesion occurred before conventional DCE-MRI. However, the researchers did not evaluate patient and tumor characteristics that may have resulted in better lesion conspicuity seen with ultrafast images. Moreover, the sample size of this previous study (n = 23) was small.

In our multivariable logistic regression analysis, premenopausal status, moderate to marked BPE, NME and shorter TTE were independently associated with better lesion conspicuity on ultrafast DCE-MRI. It is known that BPE is higher in premenopausal women than in postmenopausal women, and BPE is more prominent in

 https://doi.org/10.3348/kjr.2019.0567

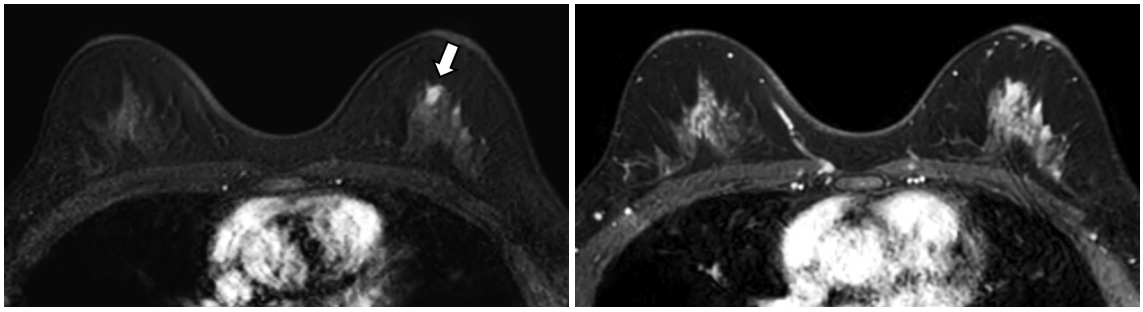

A B

Fig. 3. Preoperative breast MRI scanned using Ingenia (Philips Healthcare) in 51-year-old woman with better lesion conspicuity at ultrafast MRI.

A. 8th phase (U2) of ultrafast scan shows mass (arrow) in left upper breast. Lesion conspicuity score was 5, and lesion size was measured as 1 cm. **B.** First phase of conventional scan shows marked BPE. Due to marked BPE, mass is not clearly differentiated from background parenchyma. Lesion conspicuity score was 2, and lesion size was inaccurately measured as 2.3 cm due to marked BPE. Surgical histopathology revealed 1-cm ductal carcinoma *in situ*. BPE = background parenchymal enhancement

the first and fourth weeks and lowest in the second week of the menstrual cycle (26, 27). Hence, it would be ideal to schedule MRI examinations in accordance with each woman's menstrual cycle. However, this may not be possible in clinical situations because of the difficulties in changing surgery schedules or adding further MRI sessions. Ultrafast DCE-MRI, based on its potential usefulness in cases of high BPE, as demonstrated in our study, could be utilized for premenopausal women anticipated to have high BPE.

NME might exhibit better conspicuity at ultrafast scans because NME does not show a convex-outward contour but a discrete enhancement from the normal parenchymal enhancement. Unlike mass lesions which displace or deform surrounding anatomic structures and can be distinguished in high BPE, NME tends to be more influenced by the degree of BPE and can be more clearly distinguished with ultrafast scans. Our results agree with the previous pilot results of Jansen et al. (28) who found that high temporal resolution MRI could improve the lesion conspicuity of NME-type cancers. With regard to the association between TTE and lesion conspicuity, tumors with short TTE may show enhancement from the very early phases of ultrafast DCE-MRI when BPE is very low. Thus, tumors with short TTE might show better lesion conspicuity on ultrafast DCE-MRI.

Contrary to our initial hypothesis, the performances of ultrafast and conventional DCE-MRI for assessing tumor size were similar regardless of the level of BPE. The better conspicuity of lesions on ultrafast DCE-MRI did not lead to a statistically higher agreement with pathologic tumor size. This might be due to the extensive experience radiologists have in assessing tumor size with conventional DCE-MRI, contrary to their more limited experience with ultrafast DCE-MRI. Prior studies evaluating the performance of conventional DCE-MRI according to the level of BPE have shown that strong BPE may cause inaccurate estimations of tumor size because of lower contrast between the tumor and normal breast parenchyma (16, 18, 19). These studies only evaluated the performance of conventional DCE-MRI according to the level of BPE (16, 18, 19). However, we measured tumor size on both ultrafast and conventional scans and compared the absolute agreement between the measured tumor size with the pathologically determined tumor size, with a focus on the difference with respect to BPE level. To the best of our knowledge, there have been no studies that have compared the performances between ultrafast and conventional DCE-MRI for tumor size. Also, tumor subtype, lesion type at MRI, and TTE should be considered when assessing tumor size at ultrafast DCE-MRI, because these factors can affect the discrepancy between measured size at ultrafast DCE-MRI and histopathological size.

It should be mentioned that tumor size agreement between MRI and pathology reported in our study (ICC value of 0.63 and 0.66) was lower than the correlation between MRI and pathology reported in previous studies (Pearson or Spearman correlation coefficient = 0.65–0.98) (16, 29-31). This may be due to the differences in the statistical method (ICC is considered to be a more appropriate method to examine the size agreement than the correlation coefficient (32)) and higher proportion (14%) of DCIS cases than other studies (0–14%) (16, 29-31).

We acknowledge several limitations. First, a patient selection bias might have occurred due to the retrospective design of our single-institution study. Specifically,

https://doi.org/10.3348/kjr.2019.0567

Korean Journal of Radiology
KJR

Table 4. Factors Affecting Tumor Size Discrepancy between Pathology and MRI

Variable	Tumor Size Discrepancy between Pathology and Ultrafast MRI	*P* Value for Simple Linear Regression Analysis	*P* Value for Multiple Linear Regression Analysis	Tumor Size Discrepancy between Pathology and Conventional MRI	*P* Value for Simple Linear Regression Analysis	*P* Value for Multiple Linear Regression Analysis
Age (years)		0.246	0.198		0.547	0.776
< 40 (n = 31)	0.1 ± 1.3			0.5 ± 1.1		
≥ 40 (n = 330)	0.4 ± 1.4			0.4 ± 1.3		
Menopausal status		0.580	0.835		0.237	0.743
Premenopausal (n = 149)	0.4 ± 1.5			0.5 ± 1.4		
Postmenopausal (n = 212)	0.3 ± 1.3			0.3 ± 1.3		
Histologic type		0.109	0.333		0.991	0.739
DCIS (n = 49)	0.1 ± 1.5			0.4 ± 1.5		
Invasive carcinoma (n = 312)	0.4 ± 1.4			0.4 ± 1.3		
Histologic or nuclear grade		0.329	0.214		0.154	0.956
Low to intermediate (n = 261)	0.4 ± 1.4			0.5 ± 1.3		
High (n = 100)	0.3 ± 1.4			0.3 ± 1.4		
Tumor subtype		0.010	0.023		0.018	0.098
HR+/HER2- (n = 236)	0.5 ± 1.4			0.5 ± 1.3		
HR+/HER2+ (n = 31)	0.3 ± 1.5			0.5 ± 1.2		
HR-/HER2+ (n = 44)	-0.1 ± 1.6			0.1 ± 1.8		
Triple negative (n = 50)	0.1 ± 1.1			0.1 ± 1.0		
Lesion type at MRI		< 0.001	< 0.001		0.086	0.094
Mass (n = 288)	0.5 ± 1.2			0.5 ± 1.1		
NME (n = 73)	-0.2 ± 2.0			0.1 ± 1.9		
BPE at MRI		0.272	0.104		0.141	0.215
Minimal to mild (n = 252)	0.3 ± 1.3			0.3 ± 1.3		
Moderate to marked (n = 109)	0.5 ± 1.5			0.5 ± 1.5		
TTE (seconds)		0.011	0.006		0.412	0.268
≤ 9 (n = 229)	0.2 ± 1.5			0.3 ± 1.5		
> 9 (n = 132)	0.6 ± 1.1			0.5 ± 1.0		
Initial phase		0.670	0.187		0.747	0.330
Medium (n = 137)	0.4 ± 1.4			0.4 ± 1.3		
Fast (n = 224)	0.4 ± 1.4			0.4 ± 1.4		
Delayed phase		0.436	0.105		0.675	0.378
Persistent (n = 28)	0.5 ± 1.6			0.5 ± 1.4		
Plateau (n = 153)	0.3 ± 1.5			0.3 ± 1.3		
Washout (n = 180)	0.5 ± 1.3			0.4 ± 1.3		

Data are means ± standard deviations. Tumor size discrepancy was calculated as tumor size at surgical histopathologic examination minus tumor size at MRI. TTE was divided into two groups by cut-off of 9 seconds, median value.

women with neoadjuvant chemotherapy or women with multiple lesions at pathology were excluded in our study. Consequently, all women had unifocal cancer at pathology and 96.1% (347 of 361) of women had early stage (0 to II) breast cancer. Thus, we might not be able to generalize our study results. It would be interesting to see if women with neoadjuvant chemotherapy do not benefit from ultrafast scan in future studies, as a recent report emphasized the need for the delayed phase in these women (22). Second, lesion conspicuity can be affected by many factors, including monitor setting, window/level display setting, view angles, and the reviewers themselves. Third, BI-RADS and The European Society of Breast Imaging recommend that the center of the k-space of the first post-contrast conventional series be evaluated within 2 minutes after contrast administration in order to capture the peak enhancement of the tumor (14, 33). However, the Philips eTHRIVE took slightly longer than 2 minutes (149.5 seconds), this time lag may have reduced the contrast between the tumor and background parenchyma

 https://doi.org/10.3348/kjr.2019.0567

and consequently led to the decreased performance of the conventional scan.

In conclusion, when evaluating tumor size at preoperative breast MRI, ultrafast DCE-MRI can potentially improve lesion conspicuity compared to conventional DCE-MRI.

Conflicts of Interest

The authors have no potential conflicts of interest to disclose.

ORCID iDs

Nariya Cho
https://orcid.org/0000-0003-4290-2777
Soo-Yeon Kim
https://orcid.org/0000-0001-8915-3924
Yunhee Choi
https://orcid.org/0000-0001-5305-1803
Sung Ui Shin
https://orcid.org/0000-0001-6049-8419
Eun Sil Kim
https://orcid.org/0000-0002-0632-9902
Su Hyun Lee
https://orcid.org/0000-0001-7476-719X
Jung Min Chang
https://orcid.org/0000-0001-5726-9797
Woo Kyung Moon
https://orcid.org/0000-0001-8931-3772

REFERENCES

1. Mann RM, Mus RD, van Zelst J, Geppert C, Karssemeijer N, Platel B. A novel approach to contrast-enhanced breast magnetic resonance imaging for screening: high-resolution ultrafast dynamic imaging. *Invest Radiol* 2014;49:579-585
2. Mus RD, Borelli C, Bult P, Weiland E, Karssemeijer N, Barentsz JO, et al. Time to enhancement derived from ultrafast breast MRI as a novel parameter to discriminate benign from malignant breast lesions. *Eur J Radiol* 2017;89:90-96
3. van Zelst JCM, Vreemann S, Witt HJ, Gubern-Merida A, Dorrius MD, Duvivier K, et al. Multireader study on the diagnostic accuracy of ultrafast breast magnetic resonance imaging for breast cancer screening. *Invest Radiol* 2018;53:579-586
4. Goto M, Sakai K, Yokota H, Kiba M, Yoshida M, Imai H, et al. Diagnostic performance of initial enhancement analysis using ultra-fast dynamic contrast-enhanced MRI for breast lesions. *Eur Radiol* 2019;29:1164-1174
5. Vreemann S, Rodriguez-Ruiz A, Nickel D, Heacock L, Appelman L, van Zelst J, et al. Compressed sensing for breast MRI: resolving the trade-off between spatial and temporal resolution. *Invest Radiol* 2017;52:574-582
6. Saranathan M, Rettmann DW, Hargreaves BA, Lipson JA, Daniel BL. Variable spatiotemporal resolution three-dimensional Dixon sequence for rapid dynamic contrast-enhanced breast MRI. *J Magn Reson Imaging* 2014;40:1392-1399
7. Abe H, Mori N, Tsuchiya K, Schacht DV, Pineda FD, Jiang Y, et al. Kinetic analysis of benign and malignant breast lesions with ultrafast dynamic contrast-enhanced MRI: comparison with standard kinetic assessment. *AJR Am J Roentgenol* 2016;207:1159-1166
8. Pineda FD, Medved M, Wang S, Fan X, Schacht DV, Sennett C, et al. Ultrafast bilateral DCE-MRI of the breast with conventional Fourier sampling: preliminary evaluation of semi-quantitative analysis. *Acad Radiol* 2016;23:1137-1144
9. Onishi N, Kataoka M, Kanao S, Sagawa H, Iima M, Nickel MD, et al. Ultrafast dynamic contrast-enhanced MRI of the breast using compressed sensing: breast cancer diagnosis based on separate visualization of breast arteries and veins. *J Magn Reson Imaging* 2018;47:97-104
10. Mori N, Abe H, Mugikura S, Takasawa C, Sato S, Miyashita M, et al. Ultrafast dynamic contrast-enhanced breast MRI: kinetic curve assessment using empirical mathematical model validated with histological microvessel density. *Acad Radiol* 2019;26:e141-e149
11. Kim Y, Kim SH, Song BJ, Kang BJ, Yim KI, Lee A, et al. Early prediction of response to neoadjuvant chemotherapy using dynamic contrast-enhanced MRI and ultrasound in breast cancer. *Korean J Radiol* 2018;19:682-691
12. Ko ES, Morris EA. Abbreviated magnetic resonance imaging for breast cancer screening: concept, early results, and considerations. *Korean J Radiol* 2019;20:533-541
13. Song SE, Cho KR, Seo BK, Woo OH, Jung SP, Sung DJ. Kinetic features of invasive breast cancers on computer-aided diagnosis using 3T MRI data: correlation with clinical and pathologic prognostic factors. *Korean J Radiol* 2019;20:411-421
14. American College of Radiology. *ACR BI-RADS atlas®*, 5th ed. Reston: American College of Radiology, 2013
15. Rella R, Bufi E, Belli P, Contegiacomo A, Giuliani M, Rosignuolo M, et al. Background parenchymal enhancement in breast magnetic resonance imaging: a review of current evidences and future trends. *Diagn Interv Imaging* 2018;99:815-826
16. Baek JE, Kim SH, Lee AW. Background parenchymal enhancement in breast MRIs of breast cancer patients: impact on tumor size estimation. *Eur J Radiol* 2014;83:1356-1362
17. Park SY, Kang DK, Kim TH. Does background parenchymal enhancement on MRI affect the rate of positive resection margin in breast cancer patients? *Br J Radiol* 2015;88:20140638
18. Uematsu T, Kasami M, Watanabe J. Does the degree of background enhancement in breast MRI affect the detection and staging of breast cancer? *Eur Radiol* 2011;21:2261-2267

19. Uematsu T, Kasami M, Watanabe J. Background enhancement of mammary glandular tissue on breast dynamic MRI: imaging features and effect on assessment of breast cancer extent. *Breast Cancer* 2012;19:259-265
20. Kang JH, Youk JH, Kim JA, Gweon HM, Eun NL, Ko KH, et al. Identification of preoperative magnetic resonance imaging features associated with positive resection margins in breast cancer: a retrospective study. *Korean J Radiol* 2018;19:897-904
21. Tomida T, Urikura A, Uematsu T, Shirata K, Nakaya Y. Contrast enhancement in breast cancer and background mammary-gland tissue during the super-early phase of dynamic breast magnetic resonance imaging. *Acad Radiol* 2017;24:1380-1386
22. Kim SY, Cho N, Park IA, Kwon BR, Shin SU, Kim SY, et al. Dynamic contrast-enhanced breast MRI for evaluating residual tumor size after neoadjuvant chemotherapy. *Radiology* 2018;289:327-334
23. Santamaría G, Bargalló X, Fernández PL, Farrús B, Caparrós X, Velasco M. Neoadjuvant systemic therapy in breast cancer: association of contrast-enhanced MR imaging findings, diffusion-weighted imaging findings, and tumor subtype with tumor response. *Radiology* 2017;283:663-672
24. Hammond ME, Hayes DF, Dowsett M, Allred DC, Hagerty KL, Badve S, et al. American Society of Clinical Oncology/College of American Pathologists guideline recommendations for immunohistochemical testing of estrogen and progesterone receptors in breast cancer (unabridged version). *Arch Pathol Lab Med* 2010;134:e48-e72
25. Wolff AC, Hammond ME, Hicks DG, Dowsett M, McShane LM, Allison KH, et al. Recommendations for human epidermal growth factor receptor 2 testing in breast cancer: American Society of Clinical Oncology/College of American Pathologists clinical practice guideline update. *J Clin Oncol* 2013;31:3997-4013
26. Kuhl CK, Bieling HB, Gieseke J, Kreft BP, Sommer T, Lutterbey G, et al. Healthy premenopausal breast parenchyma in dynamic contrast-enhanced MR imaging of the breast: normal contrast medium enhancement and cyclical-phase dependency. *Radiology* 1997;203:137-144
27. King V, Gu Y, Kaplan JB, Brooks JD, Pike MC, Morris EA. Impact of menopausal status on background parenchymal enhancement and fibroglandular tissue on breast MRI. *Eur Radiol* 2012;22:2641-2647
28. Jansen SA, Fan X, Medved M, Abe H, Shimauchi A, Yang C, et al. Characterizing early contrast uptake of ductal carcinoma in situ with high temporal resolution dynamic contrast-enhanced MRI of the breast: a pilot study. *Phys Med Biol* 2010;55:N473-N485
29. Davis PL, Staiger MJ, Harris KB, Ganott MA, Klementaviciene J, McCarty KS Jr, et al. Breast cancer measurements with magnetic resonance imaging, ultrasonography, and mammography. *Breast Cancer Res Treat* 1996;37:1-9
30. Wasif N, Garreau J, Terando A, Kirsch D, Mund DF, Giuliano AE. MRI versus ultrasonography and mammography for preoperative assessment of breast cancer. *Am Surg* 2009;75:970-975
31. Luparia A, Mariscotti G, Durando M, Ciatto S, Bosco D, Campanino PP, et al. Accuracy of tumour size assessment in the preoperative staging of breast cancer: comparison of digital mammography, tomosynthesis, ultrasound and MRI. *Radiol Med* 2013;118:1119-1136
32. Koo TK, Li MY. A guideline of selecting and reporting intraclass correlation coefficients for reliability research. *J Chiropr Med* 2016;15:155-163
33. Mann RM, Kuhl CK, Kinkel K, Boetes C. Breast MRI: guidelines from the European Society of Breast Imaging. *Eur Radiol* 2008;18:1307-1318

 https://doi.org/10.3348/kjr.2019.0567